

Infrared spectroscopy techniques for studying the electronic structures of materials under high-pressure

Hidekazu Okamura*, Yuka Ikemoto¹, Taro Moriwaki¹, and Takao Nanba²

Graduate School of Science and Technology, Tokushima University, Tokushima 770-8506, Japan

¹*Japan Synchrotron Radiation Research Institute and SPring-8, Sayo, Hyogo 679-5198, Japan*

²*Graduate School of Science, Kobe University, Kobe 657-8501, Japan*

In this article, we describe our high-pressure infrared (IR) spectroscopy techniques for studying the electronic structures of materials at high pressures. High pressure of up to 20 GPa is applied to a sample using a diamond anvil cell (DAC). To accurately perform IR spectroscopy in the limited sample space of a DAC, synchrotron radiation is used as a bright IR source. Our techniques allow reflectance studies of a single crystal sample and determination of the optical functions of the sample such as dielectric function and optical conductivity. To illustrate the capability and usefulness of our techniques, some actual results of high-pressure IR studies on rare-earth compounds are described.

1. Introduction

Infrared (IR) spectroscopy has been a very useful technique used in a wide range of fields in science and engineering. Figure 1 summarizes various phenomena studied by IR spectroscopy. It also shows various spectral ranges in wavenumber (cm^{-1}), photon energy (eV), and wavelength (μm). The spectral ranges often referred to as “far IR”, “mid-IR”, and “terahertz” are also indicated, although there are no strict definitions for these ranges. As an analytical tool, IR spectroscopy has been most commonly used to study the “fingerprint” frequencies of molecular vibrations to identify various molecules and chemical bonds. In materials physics, on the other hand, it has been used to study various low-energy excitations induced by optical phonons, free carriers (Drude response), excitons, and energy gaps.^{1,2)} In particular, by using IR spectroscopy under high pressure, one can study the pressure evolution of these excitations. By applying pressure, one can also vary interatomic distance, and hence can “tune” various material parameters closely dependent on interatomic distance, such as electron bandwidth and hybridization. One can do so continuously and cleanly without introducing disor-

*E-mail: ho@tokushima-u.ac.jp

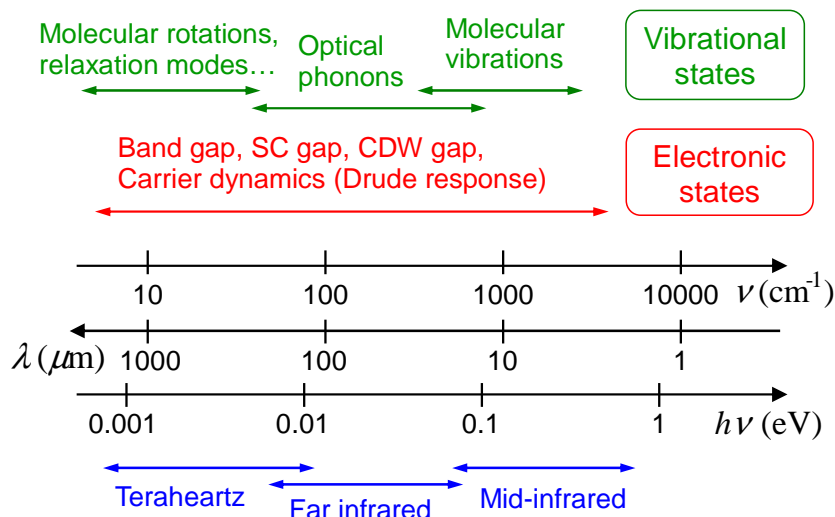


Fig. 1. (Color online) Various phenomena studied by IR spectroscopy. They are shown according to their characteristic frequencies and energies in wavenumber (ν in cm^{-1}), wavelength (λ in μm), and photon energy ($h\nu$ in eV). Also shown are technical terms for particular spectral ranges used in the text. SC and CDW represent superconducting and charge density wave, respectively.

der into a crystal, unlike in the case of chemical doping. There are other widely used spectroscopic techniques, such as photoemission and tunneling spectroscopies, that can probe the electronic structures near the Fermi level. However, these techniques cannot be used on a sample sealed in a pressure-generating cell. Therefore, IR spectroscopy has emerged as a very important tool for studying the electronic structures of a material under high pressure.

Many authors, including us, have reported high-pressure IR studies of various materials. In materials physics, for example, “strongly correlated electron systems (SCES)” have been a target of many high-pressure IR studies.³⁾ They include transition metal compounds, rare earth compounds, and organic compounds in which strong correlations among d , f , and p electrons, respectively, lead to interesting physical phenomena. Molecular solids under high pressure, such as ice,⁴⁾ dense nitrogen,⁵⁾ hydrogen,⁶⁾ and their mixtures⁷⁾ have also attracted a great deal of attention in terms of their IR studies. Another important field for high-pressure IR techniques has been earth and planetary science. Various minerals at high pressures have been studied by IR spectroscopy to understand their properties in the deep interior of the earth and other planets.⁸⁾ It is difficult to survey all the published high-pressure IR studies here, but some of the works on SCES materials have been reviewed elsewhere.³⁾ In addition, high-pressure IR instrumentations developed by different groups have been reported.^{9–14)}

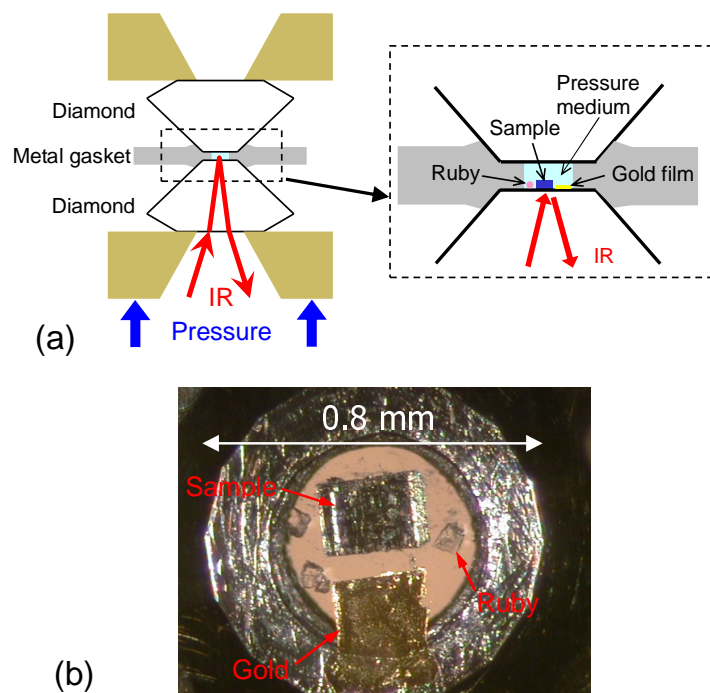


Fig. 2. (Color online) (a) Schematic illustration of IR reflectance study with a DAC. (b) Example of a sample mounted in a DAC. A gold film and ruby pieces are also mounted with the sample, with KBr used as the pressure medium.

In this paper, we will describe our own high-pressure IR techniques that we have developed over the last decade. In our technique, a diamond anvil cell (DAC) is used to apply a high pressure on a sample.^{15,16)} To accurately perform spectroscopy with long-wavelength IR radiation in the restricted sample space of a DAC, synchrotron radiation (SR) is used as a bright IR source at the IR beamline BL43IR of SPring-8,^{17,18)} which is a large-scale SR facility in Japan.

2. High-pressure IR spectroscopy with DAC

In this section, we will describe our methods to measure the reflectance spectrum $R(\omega)$ of a sample contained in a DAC. (Methods for obtaining the optical functions of a material at ambient pressure have been discussed elsewhere.¹⁹⁾ By measuring $R(\omega)$, one can derive the optical functions such as optical conductivity by Kramers-Kronig analysis or spectral fitting. With a DAC, it may be easier to measure transmission spectra of powder samples, but it is generally difficult to derive the optical functions with powder samples. (If one needs only the pressure dependence of phonon peak energy or energy gap width, a measurement of powder samples is still quite useful.) Figure 2 schematically shows the reflectance measurement with a DAC. The surface of a single

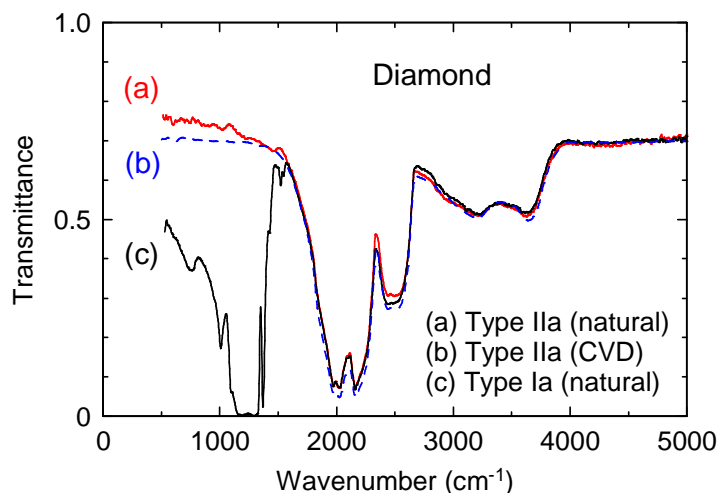


Fig. 3. (Color online) IR transmittance spectra of type Ia and type IIa natural diamond anvils with a thickness of 1.7 mm, and that of a type IIa synthetic diamond plate with a thickness of 2.2 mm, grown by CVD. All the spectra were measured at room temperature.

crystal sample is placed in direct contact with the culet surface of a diamond anvil. Since diamond is almost transparent in IR as discussed later, one can measure $R(\omega)$ in this manner. A gold film is also placed in the DAC as a reference to normalize the reflection spectrum. Small ruby pieces are used as the pressure sensor via the standard ruby fluorescence technique.^{15,16)} The space containing the sample, gold film, and ruby is filled up with a pressure-transmitting medium. (When a liquid pressure medium is used, the gold film is placed between the diamond and the gasket.) Below, the diamond, pressure-transmitting medium, gasket, and sample preparation and loading into DAC are separately discussed.

2.1 Diamond anvils

Mainly two types of diamonds, namely, types Ia and IIa, are used as anvils for high-pressure experiments.^{15,16)} The former type contains much more nitrogen impurities ($\sim 0.1\%$) than the latter type ($\ll 1$ ppm). Figure 3 shows the transmittance spectra of the two types of diamonds. Type Ia diamond shows an additional, strong absorption below 1500 cm^{-1} not seen for type IIa, which is due to the nitrogen impurities. Therefore, if the spectral range below 1500 cm^{-1} is to be studied, type IIa anvils are highly preferred. (Note that, for a reflectance study, only one of the two anvils needs to be of type IIa.) The broad absorption seen over the $1500\text{--}4000\text{ cm}^{-1}$ range is due to two-phonon absorption, and is seen for both types. The absorption at $1900\text{--}2300\text{ cm}^{-1}$ is particularly

strong, and since the light has to go through the anvil(s) twice in a DAC, this range is difficult to measure. Typically, pressures up to ~ 10 and 20 GPa can be reached with culet diameters of 800 and 600 μm , respectively.

Both natural and synthetic diamonds have been used for high-pressure studies. Recently, natural type IIa diamonds have become very difficult to obtain owing to their shortage in the international diamond market. Synthetic type IIa diamonds produced by single-crystal growth at high pressures and high temperatures have also been available, but they tend to be more expensive. More recently, however, synthetic type IIa single-crystal diamonds produced by chemical vapor deposition (CVD) have become available,²⁰⁾ which are less expensive than those produced by high-pressure single-crystal growth. In Fig 3, the transmission spectrum of a CVD-grown type IIa diamond is also shown. One can see that the CVD-grown type IIa diamond has negligible nitrogen-induced absorption, and is suited for IR studies. It is also transparent enough in the visible range, which is important in observing a sample in DAC under a microscope.

2.2 Pressure-transmitting medium

The choice of the pressure transmitting medium is very important in a high-pressure study with DAC.^{15,16)} The performance of various materials as a pressure medium has been discussed in detail.^{21,22)} As the pressure medium for IR studies, we have mainly used glycerin as the liquid medium, and KBr and NaCl as the solid media. Depending on the physical properties and surface condition of the sample, one of these is chosen. Glycerin has good properties as a pressure medium,²²⁾ i.e., it does not solidify up to 5 GPa at room temperature and has a small compressibility. A methanol-ethanol mixture is another popular liquid medium that does not solidify up to 10 GPa,²¹⁾ but caution is needed owing to its large compressibility. These liquid media generally produce more hydrostatic pressure than solid media even after their solidification at low temperatures. Although these liquid media have strong absorption in the IR region, it does not matter for reflectance studies as long as the contact between the sample and diamond is close enough. Of course, the use of liquid He, Ar, or N_2 as the pressure medium provides a much higher hydrostaticity,²¹⁾ but they generally require a cryoloading into the DAC, which is technically more demanding.

Solid media such as KBr and NaCl, although they are soft solids, produce less hydrostatic pressure than the liquid medium. However, they easily allow a clean and direct contact between the sample and diamond. With liquid medium, in contrast, it is

more difficult to maintain a close enough contact. If a thin gap exists between the sample surface and diamond, it may alter the measured $R(\omega)$ owing to interference between the light reflected from the sample surface and that from the diamond surface. This may require complicated data analysis, as actually done previously.^{23,24)} Accordingly, we now normally use KBr or NaCl rather than a liquid medium,²⁵⁾ unless the physical properties of the sample to be studied is very sensitive to the hydrostaticity of the applied pressure. (One such example is the case of pressure-induced superconductor SrFe_2As_2 .²⁶⁾)

2.3 Gasket

For our studies at pressures up to 20 GPa and at temperatures below room temperatures, we have been using stainless steel (SUS 301) plates with a thickness of 260 μm . This plate is pre-indented before applying pressure, so its actual thickness during a high-pressure study is generally less than 100 μm . A clear hole for the sample space is machined with a precision drill in our study, but electrical discharge machining and laser beam machining are also used by others.

2.4 Sample preparation and loading into DAC

To accurately measure $R(\omega)$, as already stated, the sample surface must be in contact with the diamond as closely as possible; hence, the sample surface should be as flat as possible. To mount the sample in a DAC, the sample must be prepared to have a thickness of $\sim 30 \mu\text{m}$ or less and widths of 100-200 μm depending on the culet diameter. If the sample can be cleaved, it is relatively easy to prepare such a sample. If not, polishing is usually needed to prepare a thin and flat sample. This can be done, for example, by gluing the sample on a glass plate and polishing it with a sand paper. To measure an as-grown surface rather than a polished surface, one can glue the as-grown surface on a glass plate, and then polish the other side.

With solid medium, it is relatively easy to have a clean and direct contact between the sample and diamond. When using a liquid medium such as glycerin, on the other hand, we usually apply a very small amount of Apiezon M grease between the sample and diamond to keep them in contact before sealing with the medium. Their direct contact can be checked by observing a Newton ring under a microscope, by checking for an interference fringe in the measured $R(\omega)$ spectrum, and also by observing the molecular vibration absorption of the grease in $R(\omega)$. Usually, by combining these three

methods, one can estimate whether or not the sample is closely attached on the diamond.

2.5 DAC

We have been using a DAC commercially available from Diacell (now Almax-easyLab), which has been designed for both X-ray and optical studies. It is a gas-driven-type DAC, where the piston of the DAC is pushed by a metal membrane, which in turn is pressurized by He gas supplied from a cylinder. (The pressure in the DAC is controlled by adjusting the He gas pressure with a regulator.) The DAC has an accepting angle of 60 deg, which is matched by the focusing angle of the IR microscope used.

3. High-pressure IR spectroscopy apparatus using SR as a bright source

As already described above, the sample space available in a DAC is quite limited, and the sample is also small. To accurately perform IR studies with DAC, therefore, we have used SR as a bright IR source. The brightness of IR SR has been actively utilized for the past few decades, and IR beamlines have been constructed at many SR facilities worldwide. (The properties and applications of IR SR in materials research under extreme conditions, including high-pressure studies, have been reviewed elsewhere.³⁾) We have used the high-pressure IR apparatus at the IR beamline BL43IR of SPring-8 facility. Figure 4 schematically shows the apparatus, which mainly consists of a Fourier-transform IR (FTIR) spectrometer, a custom-made IR microscope, a ruby fluorescence measurement system, a cryostat, and a He gas handling system for the gas-driven DAC. The IR SR beam is input to the microscope after going through the FTIR, and focused onto the sample mounted in the DAC. The IR microscope is equipped with a pair of reflective objectives with a large working distance (WD) of 10 cm between them. The large WD was intended to provide users with a wide variety of applications; thus, the magnification of the objective (8x) is rather small compared with standard IR microscopes. However, a small spot size close to the diffraction limit can still be obtained owing to the high brightness of IR SR. This apparatus covers a wide spectral range of 120-15000 cm^{-1} (0.015-1.9 eV) by using three different detectors, namely, a Si bolometer, a HgCdTe detector, and a Si photodiode. The optical path in the microscope is purged with air after removal of water vapor and CO_2 . The laser and spectrometer to measure ruby fluorescence are connected to the microscope through optical fibers, and the fluorescence can be measured *in situ*, without having to move the DAC from the position for IR measurement.

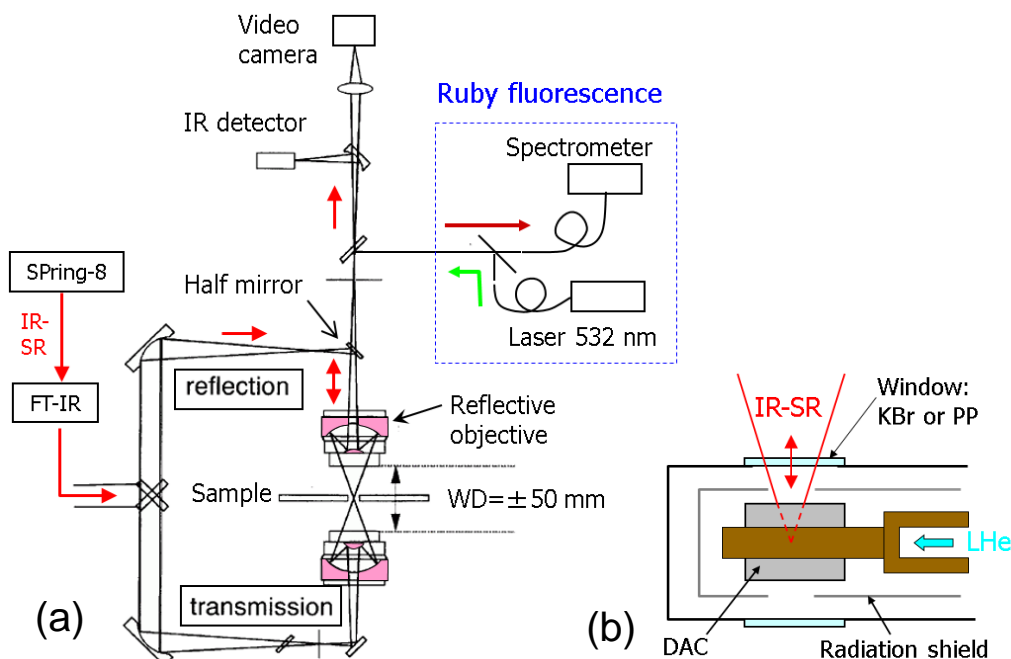


Fig. 4. (Color online) Schematic diagram of the (a) high-pressure IR apparatus at the IR beamline BL43IR of SPring-8, and (b) the cryostat used to cool the DAC.

For a low-temperature study, the DAC is mounted on the cold finger of a liquid He continuous flow cryostat as shown in Fig. 4(b), and inserted between the reflective objectives. The cryostat is mounted on a micrometer-driven XYZ stage, so that the sample position can be precisely controlled. The window for the cryostat is a KBr plate for the mid-IR, or a 0.2 mm-thick polypropylene (PP) film for the far IR. Although a PP window is deformed when the cryostat is evacuated, it can still withstand the pressure difference between the inside and outside of the cryostat. A thin stainless steel pipe is fed through the cryostat to supply pressured He gas to the metal membrane to press the DAC. This enables an *in situ* control of the sample pressure in the cryostat. However, with our gas-driven DAC, it is difficult at low temperatures to largely vary the pressure. Therefore, we usually make large pressure changes at room temperature, and then cool the DAC at a constant pressure. (It is possible to make small pressure changes even at low temperatures, if needed.)

4. Data analysis

The reflectance $[R(\omega)]$ of a sample in DAC is measured at the sample/diamond interface, unlike the usual case of the sample/vacuum or sample/air interface. Note that the refractive index of diamond in the IR range is 2.4, much greater than that of vac-

uum. According to Fresnel's formula, $R(\omega)$ at an interface between a sample and a nonabsorbing medium is expressed as^{1,2)}

$$R(\omega) = \left| \frac{n_0 - \hat{n}(\omega)}{n_0 + \hat{n}(\omega)} \right|^2 = \frac{[n_0 - n_1(\omega)]^2 + n_2(\omega)^2}{[n_0 + n_1(\omega)]^2 + n_2(\omega)^2}. \quad (1)$$

Here, $\hat{n}(\omega) = n_1(\omega) + in_2(\omega)$ is the complex refractive index of the sample, and n_0 is the refractive index of the medium, which is a real constant. Equation (1) clearly shows that there may be a large difference between the $R(\omega)$ spectra with $n_0=2.4$ (DAC) and $n_0=1$ (vacuum or air). [This is actually demonstrated later in Figs. 5(a) and 6(c).] Therefore, care must be taken in analyzing the data measured with DAC. To derive optical functions such as the optical conductivity $\sigma(\omega)$ (the real part of complex conductivity), the Drude-Lorentz (DL) spectral fitting and Kramers-Kronig (KK) analysis are widely used.^{1,2,19)} Below, the derivation of optical functions from $R(\omega)$ measured with DAC is briefly discussed.

4.1 DL spectral fitting

The DL model describe the responses of free carriers and bound electrons. In this model, the dielectric function of a material can be expressed as^{1,2)}

$$\hat{\epsilon}(\omega) = \epsilon_1(\omega) + i\epsilon_2(\omega) = \epsilon_\infty + \sum_j \frac{\omega_{p,j}^2}{\omega_{0,j}^2 - \omega^2 - i\omega\gamma_j}. \quad (2)$$

Here, $\omega_{0,j}$, $\omega_{p,j}$, and γ_j are the natural frequency, plasma frequency, and the scattering rate of the j 'th electron, respectively, and the constant ϵ_∞ represents the contribution from the higher-frequency interband transitions. For a free-carrier (Drude) contribution, ω_0 is set to zero. From the spectral fitting of a measured $R(\omega)$ spectrum using Eq. (2), the above parameters are determined, and give the dielectric function in Eq. (2). Then the refractive indices $n_1(\omega)$ and $n_2(\omega)$ can be calculated using the relations $\epsilon_1 = n_1^2 - n_2^2$ and $\epsilon_2 = 2n_1n_2$.

Figure 5 shows examples of $R(\omega)$ and $\sigma(\omega)$ calculated with the DL model. (Detailed parameters are indicated in the caption.) Here, both $R(\omega)$ spectra calculated with $n_0=2.4$ (DAC case) and $n_0=1$ (vacuum case) are shown to emphasize the large difference between them. When fitting a $R(\omega)$ spectrum measured with DAC, n_0 in Eq. (1) must be set to 2.4, but otherwise the fitting procedure is the same. Various data analysis softwares contain an automatic spectral fitting feature. For example, RefFIT²⁷⁾ software is quite useful and powerful for spectral fitting. It also allows one to set $n_0=2.4$ (or any desired value for materials other than diamond) in the fitting, a feature especially useful

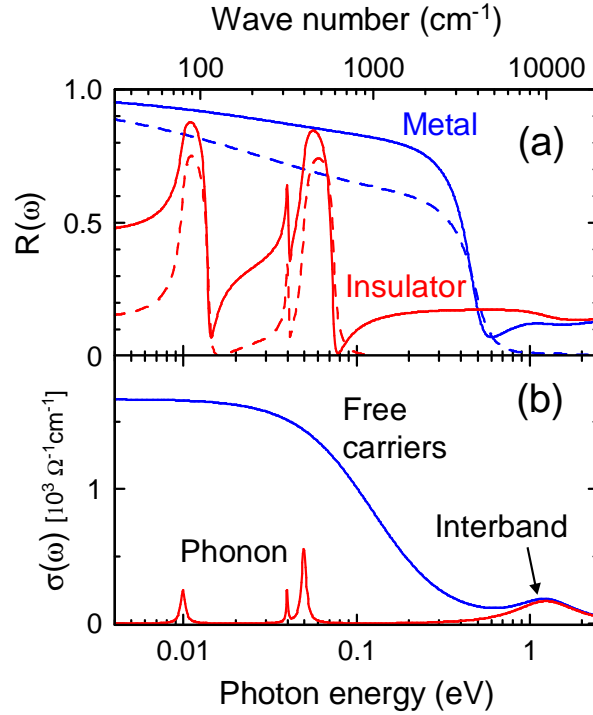


Fig. 5. (Color online) (a) $R(\omega)$ spectra given by the DL model in Eq. (2) with two sets of different parameters. The solid and broken curves are, respectively, calculated with $n_0=1$ for the vacuum case and with $n_0=2.4$ for the DAC case. The blue curves (“Metal”) simulates a metal with one Drude oscillator ($\omega_p=10000 \text{ cm}^{-1}$, $\gamma=1000 \text{ cm}^{-1}$), one Lorentz oscillator ($\omega_0=\gamma=10000 \text{ cm}^{-1}$), and $\epsilon_\infty = 5$. The red curves (“Insulator”) simulates an insulator with three Lorentz oscillators for phonons ($\omega_0=80, 320,$ and 400 cm^{-1} with $\gamma=6, 8,$ and 30 cm^{-1} , respectively) and also the same Lorentz oscillator at 10000 cm^{-1} , as in the metal case. (b) $\sigma(\omega)$ spectra given by the same parameters as in (a), showing the characteristic spectral components due to free carriers (Drude response), phonons, and interband transition.

for analyzing $R(\omega)$ measured with DAC.

4.2 KK analysis

The complex reflectivity is expressed as

$$\hat{r}(\omega) = \frac{n_0 - \hat{n}(\omega)}{n_0 + \hat{n}(\omega)} = r(\omega) \cdot e^{i\theta(\omega)}. \quad (3)$$

Here, $\theta(\omega)$ is the phase shift upon reflection, and $r(\omega) = \sqrt{R(\omega)}$ is the amplitude reflectivity of the electric field. In a conventional reflectance study, $R(\omega) = r(\omega)^2$ can be measured, and $\theta(\omega)$ in general cannot be measured. However, $\theta(\omega)$ is related to $r(\omega)$ through the KK relation as^{1,2)}

$$\theta(\omega) = -\frac{2\omega}{\pi} P \int_0^\infty \frac{\ln r(\omega')}{\omega'^2 - \omega^2} d\omega', \quad (4)$$

Here, P stands for the principal value of the complex analysis. By performing the integral in Eq. (4) with the measured $r(\omega) = \sqrt{R(\omega)}$, $\theta(\omega)$ can be obtained. In doing so, since it is impossible to actually measure $R(\omega)$ from $\omega=0$ to ∞ , extrapolations are made below and above the measured frequency range. Then, a comparison between the real and imaginary parts of Eq. (3) give $n_1(\omega)$ and $n_2(\omega)$ as

$$n_1(\omega) = \frac{1 - r(\omega)^2}{1 + r(\omega)^2 + 2r(\omega) \cos \theta(\omega)} \cdot n_0, \quad (5)$$

$$n_2(\omega) = \frac{-2r(\omega) \sin \theta(\omega)}{1 + r(\omega)^2 + 2r(\omega) \cos \theta(\omega)} \cdot n_0. \quad (6)$$

Once $n_1(\omega)$ and $n_2(\omega)$ are thus obtained, all the other optical functions such as $\sigma(\omega)$ can be derived from them.^{1,2)} Then, it may appear possible to obtain $\theta(\omega)$ even from $R(\omega)$ measured with DAC by setting $n_0=2.4$ in Eqs. (5) and (6), and to obtain \hat{n} , $\hat{\epsilon}$, and $\sigma(\omega)$. In reality, however, for a medium with $n_0 > 1$, the KK relation itself is modified, and should be given as²⁸⁾

$$\theta(\omega) = -\frac{2\omega}{\pi} P \int_0^{\infty} \frac{\ln r(\omega')}{\omega'^2 - \omega^2} d\omega' + \Delta\theta(\omega). \quad (7)$$

Here, the extra phase factor $\Delta\theta(\omega)$ depends on both the sample and medium. It is generally difficult to know the precise form of $\Delta\theta(\omega)$. The integral in Eq. (7) for $n_0 > 1$ case has been actually performed with some approximations.²⁹⁾

Alternatively, we have found a simple method based on the conventional KK relation in Eq. (4) to derive $\theta(\omega)$ from $R(\omega)$ measured with DAC.³⁰⁾ In this method, an $R(\omega)$ spectrum measured with DAC is cut off at a certain photon energy $\hbar\omega_c$, above which an extrapolation of the form ω^{-4} is applied. ω_c is chosen so that $\sigma(\omega)$ given by the above $R(\omega)$ relative to diamond (with cut off) and Eq. (4) agrees with the $\sigma(\omega)$ given by the $R(\omega)$ measured in vacuum (without cut off) and Eq. (4).³⁰⁾ With this method, $\sigma(\omega)$ can be obtained over a limited spectral range, typically below 1 eV. (The valid range depends on the material studied.)

In addition, “KK-constrained variational fitting”³¹⁾ may be used to obtain optical functions from $R(\omega)$ measured with DAC. This method is basically a many-oscillator fitting, but it can essentially perform KK analysis. The KK constrained variational fitting is included in the RefFIT software mentioned above,²⁷⁾ and can be used to perform KK analysis of $R(\omega)$ measured with DAC to obtain $\sigma(\omega)$. In this case, n_0 in Eq. (1) must be set to 2.4 to take into account the refractive index of diamond, but the modified KK relation of Eq. (7) is not needed. This method has been used in a

high-pressure IR study of a topological insulator, BiTeI.³²⁾

5. Example 1: Pressure-induced semiconductor-metal transition in YbS

As the first example, we will discuss an IR study of pressure-induced semiconductor-metal transition in YbS, where $\sigma(\omega)$ is studied at high pressures up to 20 GPa and at photon energies of 0.018-1.1 eV.³³⁾ The study was conducted at room temperature, and $R(\omega)$ measured with DAC was analyzed by DL fitting as described above.

YbS at ambient pressure is an ionic ($\text{Yb}^{2+}\text{S}^{2-}$) insulator with the rock salt crystal structure and a band gap of about 1.4 eV.³⁴⁾ The $4f$ shell is filled up with 14 electrons in the divalent Yb with no magnetic moment. Above 10 GPa, however, the average Yb valence gradually increases from 2 and reaches about 2.4 at 20 GPa, according to lattice parameter and X-ray absorption studies.³⁵⁾ A previous reflectance study made at photon energies above 0.5 eV showed that the energy gap of YbS decreased with increasing pressure and it would close at approximately 10 GPa.³⁴⁾ However, owing to a lack of measured data below 0.5 eV, detailed information about the electronic structures near the Fermi level at high pressures had not been available. We performed an IR study of YbS in a wider photon energy range of 0.02 - 1.1 eV up to 20 GPa to clarify its electronic structures under high pressure.³³⁾

Figure 6(a) shows the reflectance spectra of YbS at high pressures measured with DAC. At 0.3 GPa, $R(\omega)$ is very similar to that at ambient pressure. $R(\omega)$ is low except for the optical phonon peak near 20 meV. However, $R(\omega)$ increases markedly with pressure above 8 GPa, and the phonon peak disappears. The high-reflectance band in $R(\omega)$ is clearly due to a plasma reflection, namely, due to the Drude response of free carriers. This result clearly demonstrates that YbS is metallic at pressures above 10 GPa. In addition, $R(\omega)$ shows remarkable structures at approximately 0.15 and 0.5 eV. Figure 6(b) shows the results of Drude-Lorentz fitting analysis of the measured $R(\omega)$ spectra in Fig. 6(a). It is seen that the DL fitting has well reproduced the overall pressure evolution of $R(\omega)$. Figure 6(c) shows the reflectance spectra expected in vacuum, calculated with parameters given by the fitting in Fig. 6(b). The spectra in Fig. 6(c) show marked differences from those in Fig. 6(b), and show the non-negligible effect of diamond refractive index on $R(\omega)$ measured with DAC.

Figure 7 shows the optical conductivity $\sigma(\omega)$ obtained from the DL fitting in Fig. 6. Here, the spectrum indicated as “0” was obtained with the conventional KK analysis of $R(\omega)$ measured at ambient pressure, without using a DAC. The peak near 1.4 eV is due

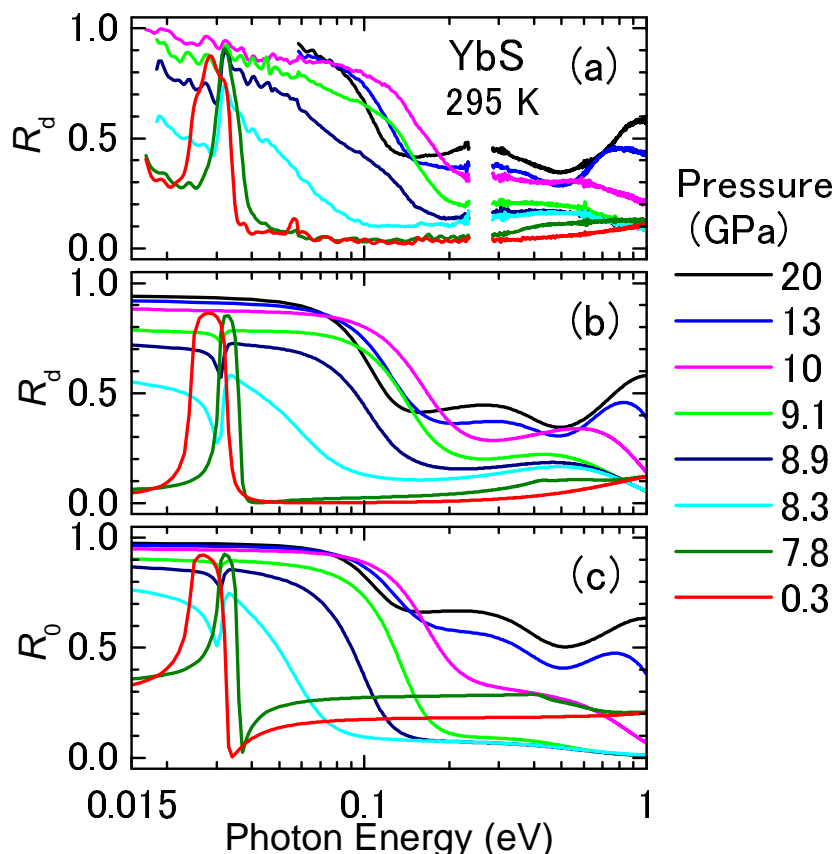


Fig. 6. (Color online) (a) Reflectance spectra of YbS (R_d) at room temperature and at high pressures measured with DAC. The spectral range where diamond has strong absorption is not indicated. Note that the measured R_d is relative to diamond, and is not relative to vacuum. (b) Results of Drude-Lorentz fitting to the measured spectra in (a). (c) Reflectance spectra of YbS relative to vacuum (R_0) given by the fitting shown in (b). From Matsunami et al.³³⁾

to the optical excitation across the band gap, showing that the band gap at ambient pressure is about 1.4 eV. With increasing pressure, this peak is seen to shift to a lower energy, indicating that the gap decreases with pressure. At approximately 8 GPa the gap closes, and above 8 GPa a Drude peak due to free carriers grows below 0.1 eV, showing the metallization of YbS. Above 10 GPa, two higher-energy peaks appear in $\sigma(\omega)$ at 0.25 and 0.8 eV. The pressure evolution, namely, the progressive gap closing, the appearance of Drude peak and the growths of the higher-energy peaks can be explained on the basis of crossing/anticrossing between a Yb 5*d*-derived conduction band and a flat 4*f* band, as previously discussed in detail.³³⁾

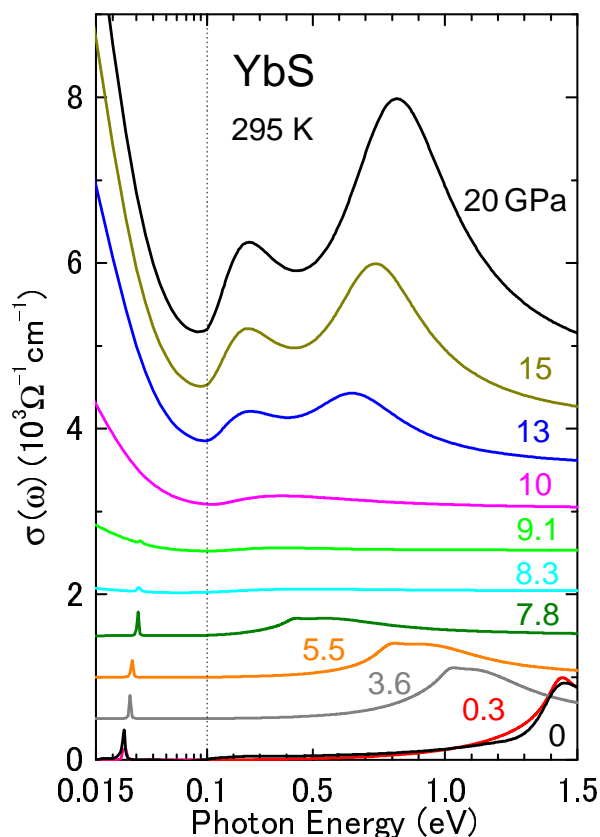


Fig. 7. (Color online) (a) Optical conductivity spectra of YbS at high pressures, obtained by the DL fitting to the measured R_d shown in Fig. 6. The spectrum indicated as “0” was given by the KK analysis of R_0 measured at ambient pressure, without using DAC. From Matsunami et al.³³⁾

6. Example 2: Pressure-induced insulator-metal transition in $\text{PrRu}_4\text{P}_{12}$

As the second example, we will discuss an IR study of electronic structures in $\text{PrRu}_4\text{P}_{12}$ under high pressure.³⁶⁾ In this work, the temperature range is from 295 to 8 K, the pressure range is from ambient to 14 GPa, and the photon energy range is from 15 meV to 1 eV. The high-pressure IR study was mainly carried out at SPring-8, but additional far-IR study was carried out at the IR beamline U2A of the National Synchrotron Light Source in the USA.³⁷⁾ In deriving $\sigma(\omega)$ from the $R(\omega)$ measured with DAC, the modified KK analysis discussed earlier was used, taking into account the refractive index of diamond.

$\text{PrRu}_4\text{P}_{12}$ is one of the compounds having the “filled skutterudite” crystal structure. Under ambient pressure, it is a metal at room temperature, but upon cooling below 63 K, it shows a metal-insulator (MI) transition with a rapid increase in electrical resistivity.³⁸⁾ In $\text{PrRu}_4\text{P}_{12}$, a Pr_{3+} ion has a large coordination number since it is located at the center of a P_{12} cage. The resulting strong hybridization between Pr 4*f* electrons and P

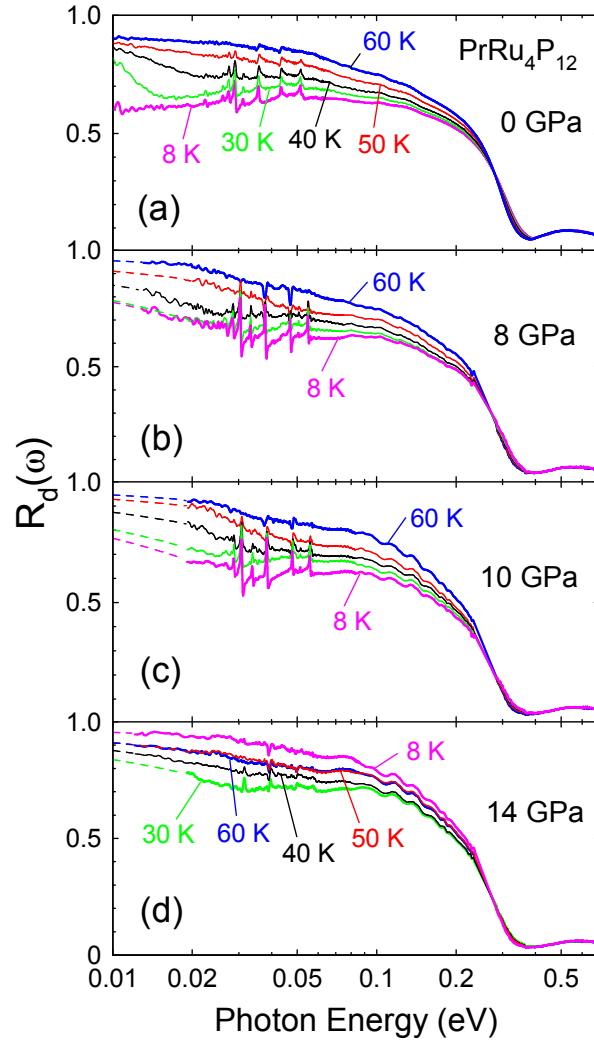


Fig. 8. (Color online) Reflectance spectra ($R_d(\omega)$) of $\text{PrRu}_4\text{P}_{12}$ at 0, 8, 10, and 14 GPa. In (a), the data were measured in vacuum without using a DAC, but $R(\omega)$ spectra expected at a sample/diamond interface are shown for comparison with the data in (b)-(d), which were actually measured with DAC. The broken curves show the low-energy extrapolations used for the KK analysis. From Okamura et al.³⁶⁾

$3p$ conduction electrons, combined with a strong nesting tendency caused by a nearly cubic Fermi surface, is believed to play an important role in this MI transition. Under increasing pressure, on the other hand, this MI transition is gradually suppressed, and above 12 GPa the resistivity again shows metallic behavior below 50 K.³⁹⁾ We performed IR study of $\text{PrRu}_4\text{P}_{12}$ at these pressure and temperature ranges to probe the electronic structures.

Figure 8 shows the $R(\omega)$ spectra of $\text{PrRu}_4\text{P}_{12}$ measured at pressures of 0, 8, 10, and 14 GPa. At ambient pressure and above 60 K, $R(\omega)$ shows metallic characteristics.

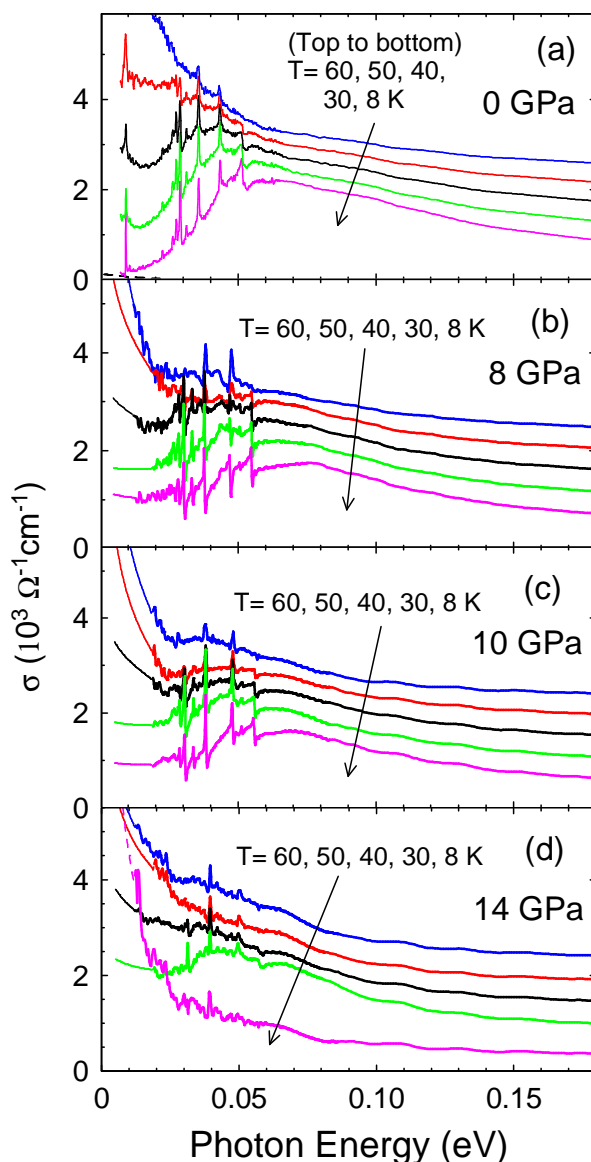


Fig. 9. (Color online) Optical conductivity spectra of $\text{PrRu}_4\text{P}_{12}$ at high pressure and low temperatures, derived from the $R(\omega)$ spectra in Fig. 8 using the modified KK analysis discussed in the text. The spectra are vertically offset for clarity. From Okamura et al.³⁶⁾

Namely, $R(\omega)$ has a clear plasma edge near 0.4 eV, below which it is high and close to 1. Upon cooling below 60 K, $R(\omega)$ decreases rapidly and sharp phonon structures appear as a result of the MI transition. At 8 and 10 GPa, the $R(\omega)$ spectra are still qualitatively similar to those at ambient pressure. At 14 GPa, however, the temperature dependence of $R(\omega)$ is quite different, namely, $R(\omega)$ decreases with cooling from 60 to 30 K, but then it significantly increases upon further cooling to 8 K. The $\sigma(\omega)$ spectra derived from $R(\omega)$ in Fig. 8 are shown in Fig. 9. In deriving $\sigma(\omega)$ from $R(\omega)$, the

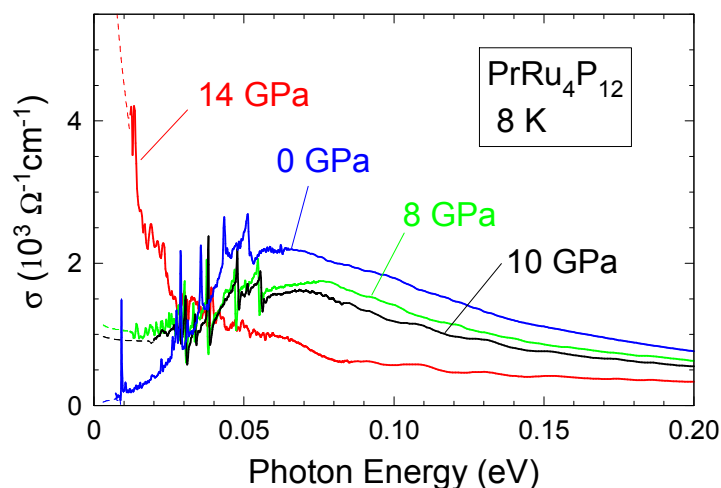


Fig. 10. (Color online) Pressure evolution of the optical conductivity (σ) of $\text{PrRu}_4\text{P}_{12}$ measured at 8 K. The broken curves show the extrapolated range. From Okamura et al.³⁶⁾

modified KK analysis discussed above³⁰⁾ was used. At ambient pressure, $\sigma(\omega)$ below 50 meV is rapidly depleted with cooling, and the opening of an energy gap is evident. From the onset of $\sigma(\omega)$ at 8 K, the energy gap width is estimated to be about 10 meV, which is in good agreement with that given by the resistivity measurement.³⁸⁾ At 8 and 10 GPa, $\sigma(\omega)$ still shows a depletion of spectral weight below 10 meV with cooling, but the gap is less developed than that at ambient pressure. This shows that the gap is partly suppressed at 8 and 10 GPa. At 14 GPa and 8 K, $\sigma(\omega)$ no longer shows an energy gap, and it sharply increases with decreasing energy. This is a Drude response of free carriers, indicating that $\text{PrRu}_4\text{P}_{12}$ is a metal. Interestingly, $\sigma(\omega)$ at 30 K still shows a gap-like feature below 50 meV, but this feature disappears with further cooling to 8 K. This result is consistent with that of resistivity, which slightly increases below 50 K and then decreases with cooling.³⁹⁾ This agreement between the spectroscopic and transport results demonstrates that our high-pressure IR study has successfully clarified the microscopic electronic structures. Finally, to show the pressure suppression of the energy gap more clearly, $\sigma(\omega)$ spectra measured at 8 K and at different pressures are shown in Fig. 10. It is interesting to note that the suppression of the energy gap with increasing pressure in Fig. 10 is qualitatively similar to that with increasing temperature in Fig. 9(a).

7. Conclusions

We have reviewed our high-pressure IR spectroscopy techniques, where a DAC is used to generate high pressures. The instrumentation and data analysis methods have been discussed, and examples of actual experiments on YbS and PrRu₄P₁₂ have been presented. To perform an IR study with a DAC, where the available sample space is quite small and confined, we have used synchrotron radiation as a bright IR source. This has made it possible to accurately measure the reflectance of a sample in both far and mid-IR ranges with a DAC. In principle, similar measurements may be carried out using a conventional IR source contained in a commercial FTIR spectrometer. However, the conventional source, which utilizes the black body radiation from a heated object, has a very low brightness. Accordingly, with a conventional IR source, it is not easy to accurately measure the reflectance of a sample in a DAC. This is even more so for low-temperature studies in which the DAC is in a cryostat and accessed through an optical window. In this regard, IR synchrotron radiation is a quite useful tool for performing an IR study under high pressure.

Acknowledgments

Part of the work at SPring-8 was carried out under approval from JASRI (2009A0089 through 2013B0089). The IR studies of YbS and PrRu₄P₁₂ were carried out in collaboration with M. Matsunami, A. Ochiai, H. Sugawara, H. Sato, C. Sekine, Z. Liu, and G. L. Carr. The financial support from JSPS KAKENHI (Grant Numbers 26400358, 23540409, and 21102512) is acknowledged.

References

- 1) M. Dressel and G. Grüner, *Electrodynamics of Solids* (Cambridge University Press, Cambridge, U.K., 2002).
- 2) G. Burns, *Solid State Physics* (Academic Press, San Diego, CA, 1985), Chap. 13.
- 3) S. Kimura and H. Okamura, *J. Phys. Soc. Jpn.* **82**, 021004 (2013).
- 4) See, for example, K. Aoki, H. Yamawaki, M. Sakashita, and H. Fujihisa, *Phys. Rev. B* **54**, 15673 (1996) and references therein.
- 5) See, for example, A. F. Goncharov, E. Gregoryanz, H.-k Mao, Z. Liu, and R. J. Hemley, *Phys. Rev. Lett.* **85** 1262 (2000) and references therein.
- 6) See, for example, C. Zha, Z. Liu, M. Ahart, R. Boehler, and R. J. Hemley, *Phys. Rev. Lett.* **110**, 217402 (2013) and references therein.
- 7) See, for example, D. K. Spaulding, G. Weck, P. Loubeyre, F. Datchi, and P. Dumas, *Nat. Commun.* **5**, 5739 (2014) and references therein.
- 8) See, for example, M. Koch-Müller, S. Jahn, N. Birkholz, E. Ritter, and U. Schade, *Phys. Chem. Miner.* **43**, 545 (2016) and references therein.
- 9) K. Syassen and R. Sonnenschein, *Rev. Sci. Instrum.* **533**, 644 (1982).
- 10) T. Nanba, *Nuovo Cimento* **20**, 397 (1988).
- 11) R. J. Hemley, A. F. Goncharov, R. Lu, V. V. Struzhkin, M. Li, and H. K. Mao, *Nuovo Cimento* **20**, 539 (1988),
- 12) R. Beyer and M. Dressel, *Rev. Sci. Instrum.* **86**, 053904 (2015).
- 13) M. K. Tran, J. Levallois, A. Akrap, J. Teyssier, A. B. Kuzmenko, F. Levy-Bertrand, R. Tediosi, M. Brandt, P. Lerch, and D. van der Marel, *Rev. Sci. Instrum.* **86**, 105102 (2015).
- 14) A. Voutea, M. Deutscha, A. Kalinkoa, F. Alabarsea, J.-B. Brubacha, F. Capitania, M. Chapuisa, V. Ta Phuoc, R. Sopracasec, and P. Roy, *Vib. Spectrosc.* **86**, 17 (2016)
- 15) S. Klotz, in *High Pressure Physics*, ed. J. Loveday (CRC Press, Boca Raton, FL, 2012), Chap. 1.
- 16) *Koatsugijutsu Handobukku* (High Pressure Technology Handbook), ed. N. Mori, K. Murata, Y. Uwatoko, and H. Takahashi (Maruzen, Tokyo, 2007) [in Japanese], Chap. 1.
- 17) Y. Ikemoto, T. Moriwaki, T. Hirono, S. Kimura, K. Shinoda, M. Matsunami, N. Nagai, T. Nanba, K. Kobayashi, and H. Kimura, *Infrared Phys. Technol.* **45** 369

- (2004).
- 18) Y. Ikemoto and T. Moriwaki, *Infrared Phys. Technol.* **51**, 400 (2008).
 - 19) H. Okamura, in *Optical Techniques for Solid State Materials Characterization*, ed. R. Prasankumar and A. J. Taylor (CRC Press, Boca Raton, FL, 2011), Chap. 4.
 - 20) Those “type IIa” CVD-grown diamonds may contain more nitrogen impurities of the order of 1 ppm than the natural type IIa ones do. However, the nitrogen-induced absorption in the IR transmittance spectrum of the CVD-grown type IIa diamond is as low as that of a natural type IIa, as discussed in the text and shown in Fig. 3. Therefore, the CVD diamond here is simply referred to as type IIa, regardless of the actual nitrogen impurity concentration.
 - 21) N. Tateiwa and Y. Haga, *Rev. Sci. Instrum.* **80**, 123901 (2009) and references therein.
 - 22) S. Klotz, K. Takemura, Th. Strassie, and Th. Hansen, *J. Phys.: Condens. Matter* **24**, 325103 (2012), and references therein.
 - 23) H. Okamura, R. Kitamura, M. Matsunami, H. Sugawara, H. Harima, H. Sato, T. Moriwaki, and Y. Ikemoto, *J. Phys. Soc. Jpn.* **80**, 084718 (2011).
 - 24) K. Hashimoto, R. Kobayashi, H. Okamura, H. Taniguchi, Y. Ikemoto, T. Moriwaki, S. Iguchi, M. Naka, S. Ishihara, and T. Sasaki, *Phys. Rev. B* **92**, 085149 (2015).
 - 25) In choosing between KBr and NaCl, the following properties should be taken into account. KBr is transparent in a wider spectral range (above 400 cm^{-1}) than NaCl (above 700 cm^{-1}). However, KBr undergoes a structural phase transition with increasing pressure near 2 GPa from the rock salt structure to the CsCl structure. Since the latter has a smaller lattice constant, the pressure in DAC drops upon this transition. In addition, KBr becomes opaque to the eye over a finite pressure range where this transition undergoes. For NaCl, in contrast, the corresponding transition occurs at a much higher pressure of about 30 GPa.
 - 26) H. Okamura, K. Shoji, K. Miyata, H. Sugawara, T. Moriwaki, and Y. Ikemoto, *J. Phys. Soc. Jpn.* **82**, 074720 (2013).
 - 27) A. Kuzmenko, RefFIT [<http://optics.unige.ch/alexey/reffit.html>].
 - 28) J. S. Plaskett and P. N. Schatz, *J. Chem. Phys.* **38**, 612 (1963).
 - 29) A. Pashkin, M. Dressel, and C.A. Kuntscher, *Phys. Rev. B* **74**, 165118 (2006).
 - 30) H. Okamura, *J. Phys.: Conf. Ser.* **359**, 012013 (2012).

- 31) A. Kuzmenko, *Rev. Sci. Instrum.* **76**, 083108 (2005).
- 32) M. K. Tran, J. Levallois, P. Lerch, J. Teyssier, A. B. Kuzmenko, G. Autes, O. V. Yazyev, A. Ubaldini, E. Giannini, D. van der Marel, and A. Akrap, *Phys. Rev. Lett.* **112**, 047402 (2014).
- 33) M. Matsunami, H. Okamura, T. Nanba, and A. Ochiai, *Phys. Rev. Lett.* **103**, 237202 (2009).
- 34) K. Syassen, H. Winzen, H. G. Zimmer, H. Tups, and J. M. Leger, *Phys. Rev. B*, **32**, 8246 (1985).
- 35) K. Syassen, *Physica B + C*, **139-140**, 277 (1986).
- 36) H. Okamura, N. Ohta, A. Takigawa, I. Matsutori, K. Shoji, K. Miyata, M. Matsunami, T. Nanba, H. Sugawara, H. Sato, T. Moriwaki, Y. Ikemoto, Z. Liu, and G. L. Carr, *Phys. Rev. B* **85**, 205115 (2012).
- 37) Z. Liu, J. Hu, H. Yang, H. Mao, and R. Hemley, *J. Phys.: Condens. Matter* **14**, 10641 (2002).
- 38) C. Sekine, T. Uchiumi, I. Shirotnani, and T. Yagi, *Phys. Rev. Lett.* **79**, 3218 (1997).
- 39) A. Miyake, K. Shimizu, C. Sekine, K. Kihou, and I. Shirotnani, *J. Phys. Soc. Jpn.* **73**, 2370 (2004).